ACS APPLIED MATERIALS & INTERFACES

Cross-Linked Electrospun pH-Sensitive Nanofibers Adsorbed with Temporin-Ra for Promoting Wound Healing

Fatemeh Koohzad and Ahmad Asoodeh*

Cite This: ACS Appl. Mater. Interfaces 2023, 15, 15172−15184

Read Online

ACCESS | Metrics & More | Article Recommendations | SI Supporting Information

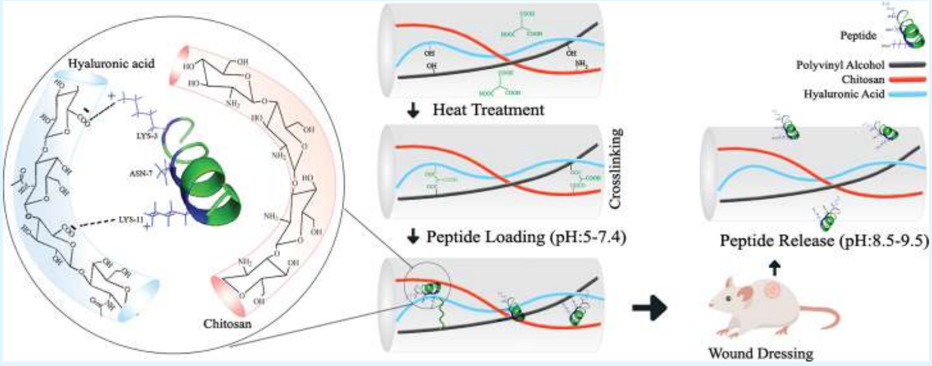

ABSTRACT: Bioresponsive nanodrug delivery systems have excellent potential in tissue engineering applications. Poly-anionic and poly-cationic biopolymers have provided a superior platform for designing pH-sensitive drug delivery systems. In this regard, hyaluronic acid−chitosan−polyvinyl alcohol complex nanofibers with high quality and reproducibility were produced by optimizing the solution preparation process. In addition, the synthesized composite nanofiber, with 66.82 kN/mm toughness, 200% swelling ratio, and 60% porosity, exhibited excellent properties to meet the requirements of the ideal wound dressing. Green cross-linking with citric acid prevented the destruction of the nanofiber even after prolonged immersion in biological solutions. ζ potential studies demonstrated that the synthesized nanofiber has a negative surface charge (~-30) at physiological pH. The pK_a of the temporin-Ra peptide is about 10, and as a result the peptide molecules have a net positive charge in physiological conditions. Therefore, peptide molecules immobilized on the synthesized scaffold based on surface adsorption. In vivo evaluation has proven that the wound bed has an alkaline environment, facilitating peptide release from the nanofiber scaffold. Electrospun nanofibers can imitate the architecture of the extracellular matrix for accelerating wound healing. In vitro investigation showed better adhesion, proliferation, migration, and fibroblast cell growth on peptide-loaded nanofiber samples than other groups. In vivo studies on full-thickness wounds in the mouse model indicated that the designed nanofiber was gradually absorbed without causing dryness or infection. On day 6, the peptide-loaded nanofiber revealed 60% wound closure compared to the control group (17%). In addition, based on histological studies, the composite nanofiber demonstrated excellent tissue repair ability, hence these active nanofiber mats can be a good alternative to existing wound dressings. Gene expression studies show that the antimicrobial peptide promotes the inflammatory phase of wound healing in a shorter time frame by accelerating the tumor necrosis factor-α cytokine response.

KEYWORDS: *pH-sensitive drug delivery, antimicrobial peptides, nanofiber, hyaluronic acid, chitosan, citric acid cross-link, wound healing*

■ INTRODUCTION

Bioresponsive materials can generate biological functions in response to pathological abnormalities.[1] The pH of the cell microenvironment is affected by different pathological conditions that can trigger controlled drug release. pH-sensitive nanomaterials are highly attractive systems for site-specific drug delivery. Among various nanomaterials for designing biomolecular delivery systems, nanofibers hold great promise in the regenerative medicine region. Regenerative medicine aims to engineer functional constructs supporting cell adherence and extracellular matrix (ECM) regeneration.

Electrospinning fabricates interconnected 3D porous scaffolds with intrinsic topographical resemblance to a native ECM that can mimic the structural and functional characteristics of an ECM.[2] At the same time, the very high surface-to-volume ratio

Received: January 3, 2023
Accepted: March 3, 2023
Published: March 20, 2023

ACS Publications

https://doi.org/10.1021/acsami.2c23268

of nanofibers leads to increased accessibility to pH-sensitive groups of biopolymers as well as drug loading efficiency.

In recent decades, biopolymer electrospinning in combination with active biomolecules has been extensively investigated to produce biomedical engineering supplies. Various electrospinning strategies have been developed for biomolecule encapsulation in electrospun nanofibers, such as co-electrospinning, co-axial electrospinning, multi electrospinning, hollow electrospinning, side-by-side electrospinning, emulsion electrospinning, and surface immobilization.[3,4]

Modern wound dressing is composed of ECM components, which not only provide structural support for cell attachment but also promote wound regeneration by triggering signaling pathways of the healing cascade.[5] Different polymers, whether natural, synthetic, or a composite of both, have been electrospun to fabricate the analogical fibrous scaffold of the ECM.[6] Anionic and cationic polymers such as hyaluronic acid (HA) and chitosan (CS) have ionizable groups that are sensitive to pH-responsive physiochemical conditions. HA, a poly-anionic polymer, is one of the components of the ECM with high hygroscopic capacities that increase during healing phases. HA modulated the entire tissue regeneration process via specific receptors, including CD44, HA-mediated motility (RHAMM), and toll-like receptors 2 and 4 (TLR2 and TLR2).[7,8] In contrast, CS, a polycationic polymer, is widely applied as tissue engineering scaffolds due to its antibacterial, antifungal, hemostatic, biodegradability, and biocompatibility features. The hemostatic property of CS arises from the electrostatic interaction between the protonated amine groups of CS and negatively charged red blood cells that promotes the stoppage of bleeding.[9] CS induces cell death by binding to the negative charge of the bacterial cell membrane and DNA, thereby altering the membrane permeability and inhibiting DNA replication.[10]

Despite the high potential of CS and HA for regenerative medicine applications, electrospinning pure polymeric solutions is difficult because of their insufficient rheological properties, high surface tension, limited solubility, and poor mechanical characteristics.[11] To overcome the electrospinning limitations of natural polymers and the repulsion forces between the charged groups, electrospinning was performed using composite nanofibers from natural and synthetic polymers.[12] Due to its high moisture retention, nontoxicity, biodegradability, chemical resistance, biocompatibility, and good fiber-forming characteristics, polyvinyl alcohol (PVA) polymer is an ideal material for tissue regeneration applications.[13]

CS, HA, and PVA are water-soluble polymers, especially at the nanoscale, and the polymeric fibers disappear as soon as they are exposed to an aqueous environment. In biomaterial design, intermolecular cross-links can stabilize nanofiber structures and control degradation rate in proportion to tissue growth. Glutaraldehyde is the most widely used component for biomaterial cross-linking; nevertheless, it is not safe for human consumption. Numerous studies report that glutaraldehyde causes chronic bronchitis, skin sensitization, and even possible genetic toxicity.[14] Carboxylic acids as green cross-linkers can provide high mechanical properties and water stability in the biomaterial. In particular, citric acid, a renewable feedstock, and a non-toxic intermediate Krebs cycle can cross-link functional groups on the neighboring polymer chains.[15]

The high potential of amphibians in the treatment of cutaneous ulcers is related to the production of a variety of wound healing peptides after injury.[16] The antimicrobial peptide promotes cutaneous tissue restoration through multiple mechanisms involving the recruitment of leukocytes, secretion of anti-inflammatory cytokines, activation of the p38 and ERK1/2 MAPK pathways, neovascularization, polarization to macrophages, cell proliferation, and migration.[17] For these reasons, peptide-loaded biomaterial is considered an ideal material for therapeutic applications.

Temporin-Ra (FP-14) is a newly discovered hydrophobic antimicrobial peptide identified and purified from the skin secretions of Rana ridibunda. These 14-amino acid non-hemolytic AMPs comprise Phe-Leu-Lys-Pro-Leu-Phe-Asn-Ala-Ala-Leu-Lys-Leu-Leu-Pro sequencing (MW: 1585.1 Da and pI 10.0).[12]

Many efforts have been made to produce CS and HA nanofibers. However, the synthesized nanofibers lack reproducibility or sufficient mechanical properties to be used in tissue engineering,[18] or the composite nanofibers were cross-linked by glutaraldehyde, which was not approved by the Food and Drug Organization.[19] In this study, a nanofibrous copolymer scaffold of CS, HA, and PVA was fabricated by the electrospinning method. We hypothesized that green cross-linked composite nanofibers would have good mechanical properties and biocompatibility for peptide loading. Peptide loading and release were done according to the difference in the surface charge of the biopolymers and the peptides in the physiological and pathological pH of the skin. Since fibroblasts are the most abundant cells in the skin tissue, in vitro biocompatibility tests were assayed using the L929 fibroblast cell. In parallel, we investigated the potential wound healing-promoting activity of each construct nanofiber with a full-thickness dermal wound in order to identify those materials that were most compatible as an active dressing for wound healing.

MATERIALS AND METHODS

Materials. HA (MW = 1500−1800 kD), CS (medium molecular weight, MW = 50−190 kD, 85% deacetylation), PVA (MW = 89−98 kD), and 2-(4-iodophenyl)-3-(4-nitrophenyl)-5-(2,4-disulfophenyl)-2*H*-tetrazolium (cell viability assay solution) were purchased from Sigma-Aldrich, Germany. Citric acid, glutaraldehyde, acetic acid, and ethanol were obtained from Merck, Germany. RPMI-1640 and fetal bovine serum (FBS) were obtained from Gibco, USA. Penicillin and streptomycin (Pen−Strep) were purchased from Biosera, USA. L929 murine fibroblastic cell line was obtained from the Research Institute of Biotechnology, Mashhad, Iran. BALB/c mice were supplied by the faculty of pharmacy, Mashad, Iran.

Temporin-Ra was synthesized by the solid-phase method (GL Biochem Shanghai Ltd., Shanghai, China) using the standard Fmoc (9-fluorenyl-methoxycarbonyl) chemistry. Synthetic peptides were subjected to reverse-phase high-performance liquid chromatography (RP-HPLC) on a C8 column (Macherey−Nagel GmbH & Co., Duren, Germany) using a linear gradient of acetonitrile (5−60% for 60 min) containing 0.1% trifluoroacetic acid at a flow rate of 2 mL/min.

EXPERIMENTAL SECTION

Optimization of the Electrospun HA−CS−PVA Nanofiber. PVA (10% w/v) and HA powder (2% w/v) were dissolved in distilled water on a stirrer at 80 and 25 °C, respectively. CS solutions (4% w/v) were prepared by dissolving CS powder in acetic acid (2% v/v). PVA and CS solutions were mixed together at a volume ratio of 50:50, 60:40, 70:30, and 80:20 to prepare a PVA−CS blended solution. PVA−HA blended solution was prepared at different volume ratios (50:50, 60:40, 70:30, and 80:20) of PVA and HA solutions.

PVA−CS and PVA−HA blended solutions were mixed at different volume ratios for the preparation of the PVA−HA−CS final solution. All solutions were stirred at room temperature for 24 h. Citric acid was added to PVA−HA, PVA−CS, and PVA−HA−CS polymer solutions in different concentrations (1, 2, 3, 4, 5, and 6% w/v) 4 h before electrospinning and during stirring. The electrospinning process was performed by a dual pump electrospinning machine (Fanavaran Nano-Meghyas, Iran). After fixing the plastic syringe (22 gauge), various values of voltage (15−28 kV), flow rate (0.5, 1, 1.5, and 2 mL/min), and collector-to-tip distance (8, 12, 16, and 20) were used for parameter optimization. To activate the cross-link agent, the nanofiber mats were heat-treated on a hot plate at 120 °C temperature for 4 h.[20,21]

Viscosity of Solutions. Dynamic viscosity of an electrospinning solution was conducted using a DV-II$^+$ rotational rheometer (Brookfield, USA). The measurements were performed at 20 different shear rates ranging from 14 to 150 s^{-1} at room temperature.

Fourier Transform Infrared Spectroscopy and X-ray Diffraction. Infrared spectra of the electrospun nanofibers before and after cross-linking were collected on a spectrometer (Thermo Nicolet 370—Avatar/USA) in a scanning range of 400−4000 cm^{-1}. To remove unreacted citric acid and non-cross-linked polymer, before infrared spectroscopy, all cross-linked nanofibers were washed three times with deionized water and then dried.

To study the crystallinity of prepared nanofibers, wide-angle X-ray diffraction (XRD) analysis was performed using a high-resolution diffractometer (Explorer, Italy) in a 5−45° 2θ range.

Thermal Analysis. The thermal characterizations of the pure materials and the electrospun mats were investigated by differential scanning calorimetry (DSC, SANAF, IRAN) under a dynamic nitrogen atmosphere. About 10 mg of each sample heated to 300 °C at a flow rate of 10 °C/min.

Tensile Test. The tensile strength of nanofiber mats was tested using the Universal Tensile Testing Machine (Santam, Iran). Tests were performed with specimens of nanofibers (30 mm × 10 mm size and 0.18−0.23 mm thickness) at a 50 N load cell and 1 mm/min crosshead speed.

Surface Hydrophilicity. To investigate the wetting behavior of nanofiber mats, an optical contact angle meter (ASCAM, Adecco, Iran) was used. The 4 μL droplets of deionized water were poured onto the surface of the nanofiber mats, and then the water contact angle was measured after 6 s.

Swelling Ratio and In Vitro Degradation. To examine the swelling kinetics of the fabricated nanofibers, the dry mats were weighed (W_d) and then immersed in PBS at 37 °C. At certain intervals, the nanofiber mats were put on filter paper to remove the excess water on the surface of the scaffolds, and then the weight of the wet nanofiber (W_s) was recorded. Use the equation to calculate the swelling ratio (SR)

$$\mathrm{SR}\ (\%) = \frac{W_s - W_d}{W_d} \times 100 \quad (1)$$

For the in vitro degradation study, the initiate weight of the mats (W_i) was recorded, and the scaffolds were wholly soaked in PBS at 37 °C. At different time intervals, the scaffolds were completely dried in a vacuum oven, and the final weight (W_f) of the dry mats was recorded precisely. The percentage of weight loss, WL (%), was calculated from the following eq 2

$$\text{weight loss}\ (\%) = \frac{W_i - W_f}{W_i} \times 100 \quad (2)$$

Porosity Measurement. Absolute ethanol liquid displacement is a reliable method for scaffold porosity assays without impelling shrinkage.[22] Electrospun nanofibers were immersed in the initial volume (V_1) of ethanol, and the final volume of the ethanol and scaffolds was recorded (V_2). The scaffold was pulled out, and the residual volumes of ethanol (V_3) were measured. The porosity was calculated by the following eq 3

$$\varphi = (V_1 - V_3)/(V_2 - V_3) \quad (3)$$

The pore size distribution of nanofibers was measured using the threshold instrument of ImageJ software.

Surface Morphology and Fiber Diameter. The morphology of nanofibers was analyzed by scanning electron microscopy (SEM, LEO VP 1450, Germany). Before observation, the surface of the nanofiber mats was coated with gold to increase their conductivity. The average nanofiber diameter was quantified using image analysis software (Image J, National Institutes of Health, Bethesda, Maryland, USA) by randomly selecting 100 fibers per SEM scaffold image. Graph Pad Prism was chosen to plot the nanofiber distribution using the calculated standard deviation (σ) and mean (μ) for the given sample size.

The miscibility of HA, CS, and PVA was checked by transmission electron microscopy (TEM, LEO 912 Ab, Zeiss Co, Germany). Nanofibers were collected over the carbon-coated copper grid, and the detailed morphology of the fiber was investigated at an accelerating voltage of 80.0 kV.

Degree of Citric Acid Cross-linking. The dry cross-linked nanofibers were weighed carefully (W_d) and placed in an ultrasonic for 10 min. Then, the nanofiber was dried at 100 °C and weighed again (W_u). The degree of cross-linking was calculated using the following equation[23,24]

$$\text{degree of cross} - \text{linking}\ (\%) = \frac{W_u}{W_d} \times 100 \quad (4)$$

Surface Charge of the Scaffold. The surface charge of PVA−HA−CS cross-linked nanofibers at different pHs was investigated through the modified ζ potential methodology.[25,26] Measurements were done by the dispersion of 0.02 g/L dry nanofiber in PBS solution using a silent homogenizer (Heidolph, Germany). Then, the resulting suspensions were filtered via Whatman filter paper (Grade 42, 110 mm diameter). The ζ potential of the filtrated suspensions was measured using a Zetasizer instrument (CAD, France).

Evaluation of Peptide Loading and Release. The peptide immobilization was conducted by electrostatic adsorption. The pieces of nanofiber (100 mg of dry fiber) were immersed in the peptide solution with a concentration of 200 μg/mL at different pH (pH = 5, 7.4, and 10), and the mixture was incubated at 25 ± 2 °C under shaking. Every 3 h, 100 μL of the solution was collected and replaced with fresh PBS to calculate the amount of peptide loading on the nanofiber. Drug loading efficiency was evaluated using the TNBSA (2,4,6-trinitrobenzene sulfonic acid) method. To achieve this aim, add a 0.01% (w/v) solution of TNBSA to the harvested sample solution, which was incubated for 2 h at 37 °C. After adding SDS (10%) and HCL (1 N), the absorption of the samples was measured at 335 nm. To eliminate non-immobilized peptides, the peptide-loaded nanofibers were removed from the solution and rinsed with deionized water. The peptide-loaded nanofibers were freeze-dried for subsequent analysis. To evaluate the peptide release from the nanofiber mats, the peptide-loaded scaffold was immersed in PBS solution (pH = 5, 7.4, and 10), and the amount of peptide release was measured at 335 nm. Quantitative determination of peptide loading and release was accomplished through comparison to a standard curve generated by using a series of known concentrations of the peptide. To plot the standard curve, a serial dilution of peptide concentration (800, 400, 200, 100, 50, 25, and 12.5 μg/mL) was prepared, and after adding the TNBS reagent and reading the absorbance of samples at 335 nm, generated standard curve of peptide concentration versus absorbance.

Cell Adhesion and Morphology Study. To investigate cell morphology and adhering on the surface of synthesized mats, the nanofiber scaffolds were sterilized by exposure to ultraviolet (UV) radiation for 60 min. Fibroblast cells with 5×10^4 density suspense in 100 μL of culture medium were seeded on nanofiber mats (10 × 10 mm^2). After 1 h incubation, the culture medium was added to cover the nanofiber mat surface. After 24 h, the cells were fixed in 2.5% glutaraldehyde for 60 min at 4 °C. Subsequently, the samples were dehydrated with incremental concentrations (25, 50, 75, 95, 99, and 100% v/v) of ethanol for 15 min each and dried under the fume hood.

Cell Viability. Cell viability and biocompatibility of synthesized nanofibers were examined by the MTT method. For this purpose, L929 fibroblast cells were cultured in a complete medium (10% FBS and 1% Pen−Strep). After three passages, an initial density of 7×10^4 cells/well of L929 was seeded on 24-well plates. The next day, the sterilized nanofibers at various concentrations (0.5, 1, and 1.5 mg/mL) were immersed in the complete cell culture medium. After 24 h incubation,

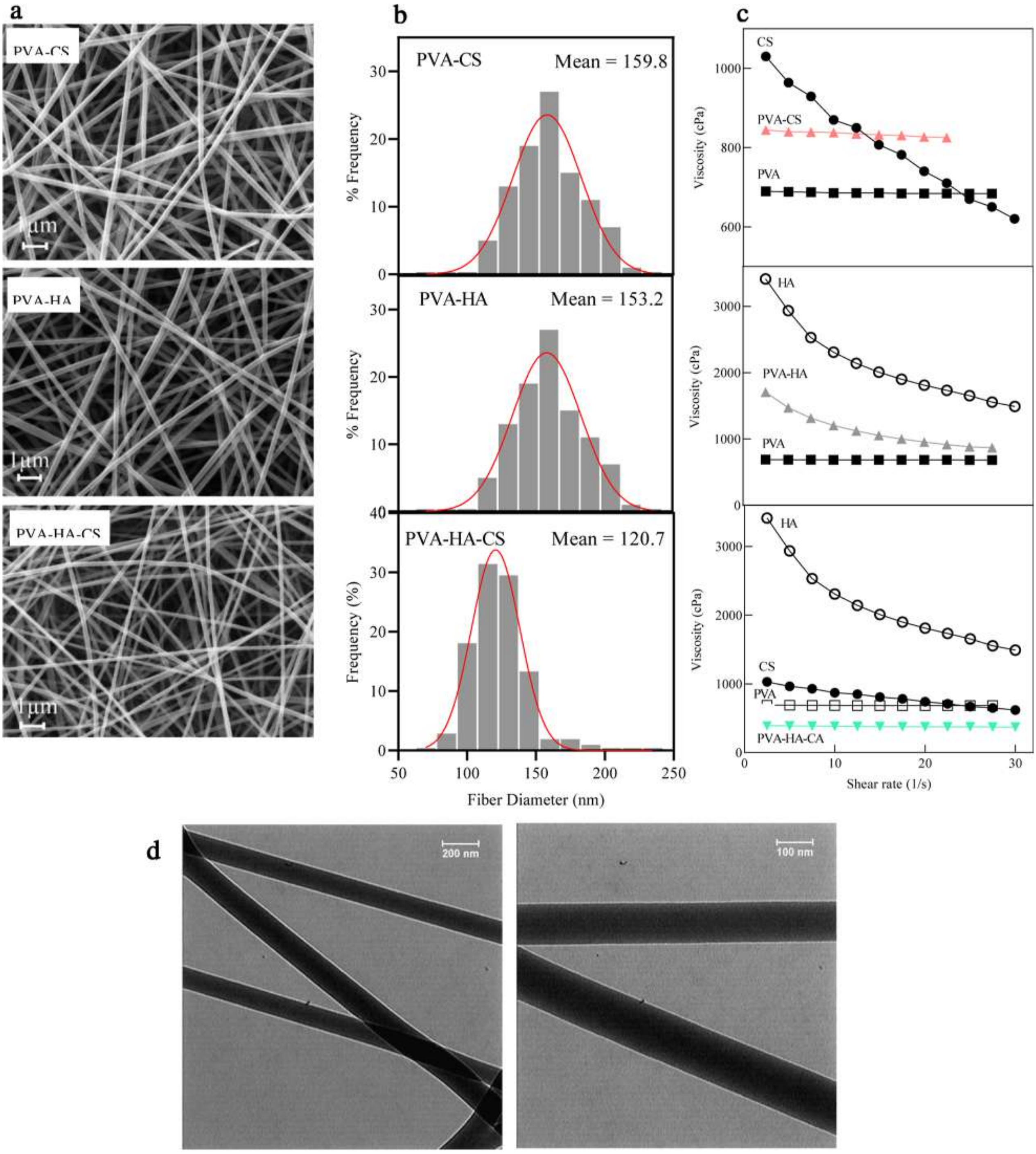

Figure 1. (a) SEM micrographs of the nanofibers prepared from precursor PVA−CS (70:30), PVA−HA (70:30), and PVA−CS + PVA−HA (50:50), (b) average fiber diameter distribution and (c) comparative plots of viscosity versus the shear rate of PVA (10%), CS (4%), HA (2%), PVA−CS (70:30), PVA−HA (70:30), and PVA−HA−CS complex solutions, (d) TEM micrographs of PVA−HA−CS nanofibers.

the cell culture medium was discarded and MTT solution was poured into each well. The well plate was incubated at 37 °C for 4 h. Afterward, DMSO was added to each well to dissolve the formazan crystals completely. After transferring the dissolved solution to a 96-well cell culture plate, the absorbance was recorded at 570 nm with a plate reader.

In Vitro Cell Migration Assay. The migration capability of L929 fibroblast cells was measured using the wound healing assay. For this purpose, cells were seeded in 24-well culture plates with 15×10^4 cells/well density and incubated to achieve a monolayer cell. After forming confluent monolayer cells, a cell-free gap area was created by scrap the cell surface in a straight line with a 100 μL pipette tip. After a scratch, to debride dead and non-adherent cells, the wells were gently washed with PBS. Then, the PBS solution was replaced with a serum-free medium containing nanofiber mat (1.5 mg/mL). Finally, the wound closure rate was monitored at different times (0, 24, and 48 h) and photographed using a light microscope. Quantification of cell migration rate was performed using ImageJ software, and the percentage of wound closure area was calculated according to the following equation

$$\%\ \text{wound closure} = \frac{\text{Xt}_0 - \text{Xt}_n}{\text{Xt}_0} \quad (5)$$

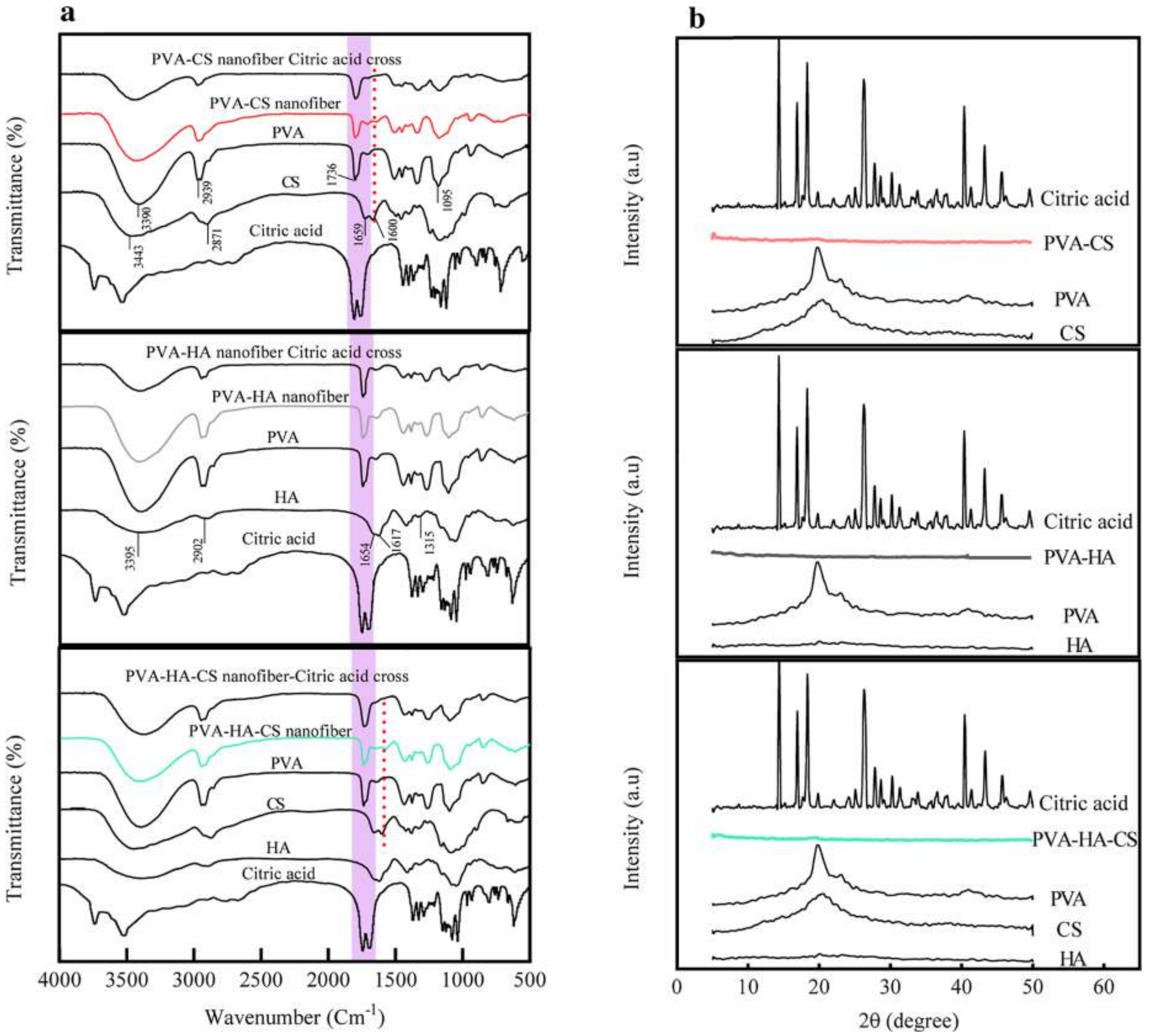

Figure 2. (a) FTIR spectra and (b) XRD patterns of pristine material in powder form and different composite nanofibers before and after cross-linking with citric acid.

where Xt_0 and Xt_n are the gap areas at zero time and specified time intervals after treatment, respectively.

In Vivo Study. Female Balb/c mice (18−23 g) were anesthetized by ketamine and xylazine hydrochloride (2.5:1.5) intraperitoneal injection. The surgical area was sterilized with alcohol, and then used a sterile 5 mm biopsy punch to create symmetrical full thickness on the dorsal skin of the mice. Silicon ring splints inside 6 mm diameter were secured with adhesive around the wound and subsequently sutured through at least six interrupted 5−0 silk sutures (Supa, Iran). The 6 mm diameter punches of nanofiber scaffold were directly inserted into the wound bed. After treatment, a sterile film dressing (Euroderm, Italy) was used to cover the wounds. Six groups, with five mice in each group (n = 5), were used for the experiments. The wound healing was recorded by measuring the wound area on days 0, 3, and 6 after the injury. The experimental protocol was approved by the Institutional Animal Ethics Committee of the Ferdowsi University of Mashhad (Document no: IR.UM.REC.1401.053).

Previous studies have shown that the pH of wounds in the early days was often alkaline.[27] To examine the pH value of the wound, the litmus strip was placed on the wound bed for 5 s, removed, wait for 30 s later, compared with the indicator scale.

Histopathological Analysis. After wound healing treatments for 6 days, the harvested skin tissue was fixed with 4% paraformaldehyde, embedded in paraffin, sectioned, and stained with Masson's trichrome. Capture images were analyzed to compare the healing rates of wounds, tissue formation, collagen deposition, and re-epithelialization for the groups. Masson's trichrome stains the collagen fiber blue. Collagen density was evaluated by color-deconvolution plugins of ImageJ software.[28]

Quantitative Real-Time Polymerase Chain Reaction Analysis of TNF-α Cytokine. To conduct real-time polymerase chain reaction (RT-PCR) analysis, the mice in the control and peptide-loaded nanofiber-treated groups were further divided into five subgroups (0, 12-, 24-, 36-, and 48 h post-injury; n = 3). Full-thickness biopsies from wounded skin sections were harvested at various time points and immediately pooled in an RNAfix solution. Then the tissue was stored at −80 °C until further usage. For RNA extraction, the frozen tissue was cut with a scalpel on a sterile Petri dish then, transferred approximately 40 mg of tissue into the tube, and added 750 μL Lysis Buffer. The tissues were homogenized by a bullet homogenizer and incubated at room temperature for 5 min. Total RNA was isolated from a homogenized skin sample using the RNA extraction kit (Parstous Co, Iran). 10 μg of total RNA was reverse transcribed into cDNA by using a first-strand cDNA synthesis kit (Parstous Co, Iran).

Quantitative RT-PCR (qRT-PCR) was performed using CFX RT-PCR Detection Systems (Bio-Rad, USA) with 40 cycles of amplification. Threshold cycles of primer were normalized to the housekeeping gene GAPDH. Primers were designed using Primer Express software (version 3.0.1.0) and are as follows: tumor necrosis factor (TNF)-α:

forward, 5′-TATGGCTCAGGGTCCAACTC-3′, and reverse 5′-CTCCCTTTGCAGAACTCAGG-3′; GAPDH: forward, 5′-TCTCCCTCACAATTTCCATCC-3, and reverse 5′-GGGTGCAGCGAACTTTATTG-3′.

RESULTS AND DISCUSSION

Electrospinning Optimization and Nanofiber SEM−TEM Analysis. To optimize the nanofiber synthesis, various parameters such as viscosity, polymer concentration ratio, citric acid concentration, voltage, distance, and flow rate were extensively studied in detail.

For PVA−CS and PVA−HA, uniform and bead-free nanofibers with the lowest fiber diameter were obtained at in the volume ratio of 70:30. In the PVA−HA−CS nanofibers, the increase in HA percentage caused the bead formation, and the rise in CS content led to the enhanced nanofiber diameter. The optimized nanofiber was produced in the volume ratio of 50:50 PVA−CS and PVA−HA blended solutions. In concentrations of more than 1% citric acid, the solution was collected at the tip of the needle, and electrospinning would not initiate because of the high viscosity. The final electrospinning parameters were selected to be a flow rate of 0.5 mL/h, a distance of 120 mm, and a voltage of 27 kV.

Beadles and uniform structures of nanofibers can be seen in the SEM images of all three types of scaffolds. The average fiber diameter in the PVA−HA−CS nanofiber scaffold was 120 nm, while in the PVA−HA and PVA−CS nanofiber scaffolds; it was 160 nm, which is significantly different (Figure 1a,b). In the case of PVA−HA−CS mate, more than 90% of fibers have a narrow diameter distribution, in the range of 100−200 nm, which is essential in planned materials for specific purposes in medical engineering.

The TEM image of PVA−HA−CS nanofiber confirms a uniformity in diameter without any phase separation between various polymers (Figure 1d).

Rheological Behavior of Solutions. The unusually high viscosity of polyelectrolyte HA polymer at even relatively low concentrations is due to the intermolecular associations between functional groups of polymer chains.[29] The non-Newtonian pseudoplastic behavior of pure CS and HA (Figure 1c) can be attributed to the chain-expanding structure and consequent increase in entanglement.[30] Meanwhile, the PVA solution exhibits Newtonian behavior. Adding PVA significantly reduced the pseudo-plasticity and viscosity of CS and HA solutions. The inter- and intra-molecular hydrogen in the polyelectrolyte polymer was disrupted by the intercalating of PVA chains. Then the hydrogen interaction among poly-ionic polymers and PVA chains was rearrangement. Reducing the viscosity of the HA−PVA−CS solution facilitates the formation of the Taylor cone.

Fourier Transform Infrared Spectroscopy. The Fourier transform infrared (FTIR) analysis method was used to identify specific molecular groups predominating in the polymer structure and how they altered due to cross-linking reactions. For PVA, the characteristic absorption peaks are at 3390 cm^{-1} (O−H stretching), 2939 cm^{-1} (asymmetric stretching of CH2), 1736 cm^{-1} (C=O vibration stretching), and 1095 cm^{-1} (C−O−C stretching).[31]

CS powder demonstrates that the band at 1600 cm^{-1} is appointed to the NH bending (amide II) (NH_2), and the small peak at 1659 cm^{-1} is associated with the C=O stretching (amide I) O=C−NHR.[32] HA shows the band at 1617 cm^{-1}, which corresponds to the amide carbon. In addition, a band at 2902 cm^{-1} is due to the C−H peak. The absorption band at 1023 cm^{-1} is attributed to the linkage stretching of C−OH.[31,33] The citric acid displayed two peaks at 1701 and 1745 cm^{-1} corresponding to C=O.

As seen in Figure 2a, all cross-linked nanofibers showed lower intensity absorbance peaks around 3500 cm^{-1}, which may be attributed to the participation of the −OH group in the cross-linking reaction. The primary amine peak at 1600 cm^{-1} (shown by a dashed line) disappeared in PVA−CS cross-linked nanofibers, which was attributed to the esterification between citric acid and CS. Increase the peak at 1740 cm^{-1}, the characteristic absorption of the C=O group in citric acid, confirms the esterification reaction between polybasic organic acid and other reacted polymers (highlighted area). These results demonstrated that cross-linking was done by esterification between carboxyl groups from citric acid and hydroxyl or amine groups from other polymers.

X-ray Diffraction. XRD is a powerful non-destructive technique used to determine the nature of the material as crystalline or amorphous.[34] As can be seen in Figure 2b, the XRD pattern of both pure CS and PVA showed a strong reflection at t $2\theta = 20.8°$, which is assigned to the crystalline motifs of linear PVA and CS molecules. The sharp peaks of PVA and CS became weak in the PVA-CS nanofibers, representing strong interactions among CS and PVA and the amorphous structures of polymers. The XRD pattern of HA exhibited humps with low-intensity peaks that characterize disordered structures. These results also revealed that electrospun fibers have a lower degree of crystallinity than the pristine materials. Indeed, the high rate of nanofiber aggregation, solvent evaporation, and elongated nanofiber solidification does not provide the time required for the crystallization of polymers. The amorphous structure of synthesized nanofibers is analogous to the ECM topography.

Thermal Behavior of Electrospun Scaffolds. DSC was performed to evaluate the impact of citric acid cross-linking on the crystallinity and thermal properties of electrospun nanofibers. Figure S1d shows the DSC curve of pure PVA, CS, HA, and citric acid. DSC curve analysis of citric acid demonstrated a strong exothermic peak at around 160 °C, which is due to the crystallization of citric acid. Likewise, an exothermic peak was also observed for pure CS and HA. As was observed in Figure 1Sa−c, the exothermic peak disappears after electrospinning. This reveals that the crystalline structure did not develop during the electrospinning process. The DSC results are in agreement with the XRD data.

Table 1 lists the thermal properties of the nanofibers before and after citric acid cross-linking. It is evident that the melting temperature (T_m) of all nanofiber mats shifts to a higher temperature after cross-linking. The increased glass transition temperature (T_g) of the PVA−HA−CS mat compared to PVA−HA and PVA−CS nanofibers provides evidence of interaction between CS and HA. An endothermic peak was observed in the

Table 1. Thermal Property of Nanofiber Mats

sample	T_g (°C)	T_m (°C)	ΔH_m (J/g)
PVA−CS	29.2	287	21.29
PVA−CS-cross-linked	35.3	302	54.05
PVA−HA	28.5	277	18.7
PVA−HA-cross-linked	34.8	301	45.12
PVA−HA−CS	72.4	280	23.4
PVA−HA−CS-cross-linked	78.1	302	57.9

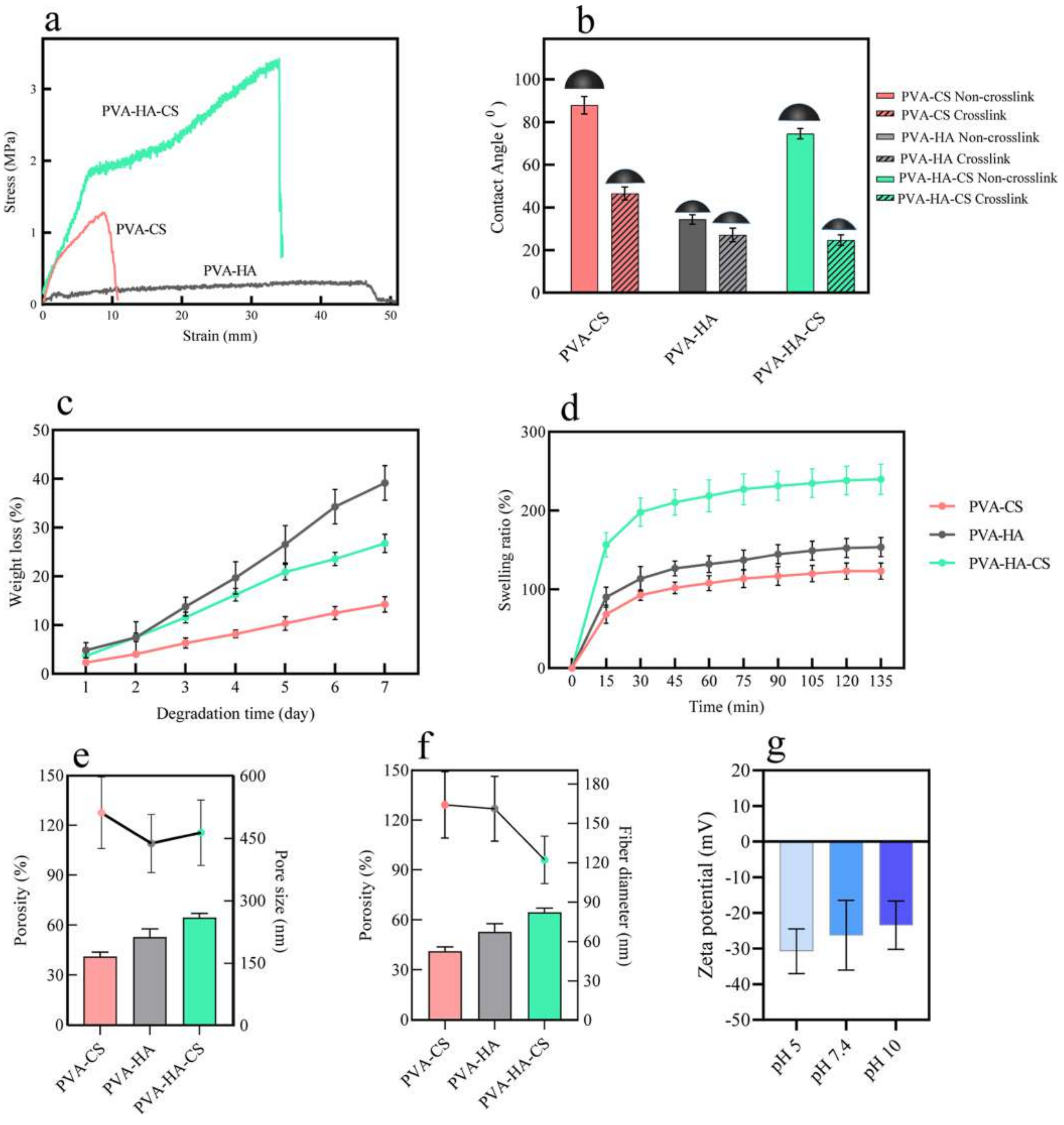

Figure 3. Physical properties of nanofibers. (a) Representative tensile stress−strain curve of the electrospun nanofibers, (b) water contact angle of nanofiber mats before and after citric acid cross-linking, (c) in vitro degradation behavior, (d) swelling ratio of electrospun scaffolds, (e) comparison of porosity versus pore size, (f) comparison of porosity versus nanofiber diameter, (g) ζ potential of PVA−HA−CS nanofiber at different pHs.

Table 2. Mechanical Property of Nanofiber Mats

sample	thickness (μm)	Young's modulus (MPa)	ultimate strength (MPa)	elongation (%)	toughness (kN/mm)
PVA−CA	50	39.2741	1.278	8.6397	9.2014
PVA−HA	20	26.54	0.3326	46.455	5.1797
PVA−HA−CS	230	42.5864	3.4378	33.544	66.82

DSC curve of nanofibers, and melting enthalpies (ΔH_m) were calculated from the area under the melting peaks. The melting enthalpy also increased with the incorporation of the cross-linking agent in nanofibers. Our study demonstrated that citric acid cross-linking significantly improves the thermal properties of the electrospun nanofibers.

https://doi.org/10.1021/acsami.2c23268
ACS Appl. Mater. Interfaces 2023, 15, 15172−15184

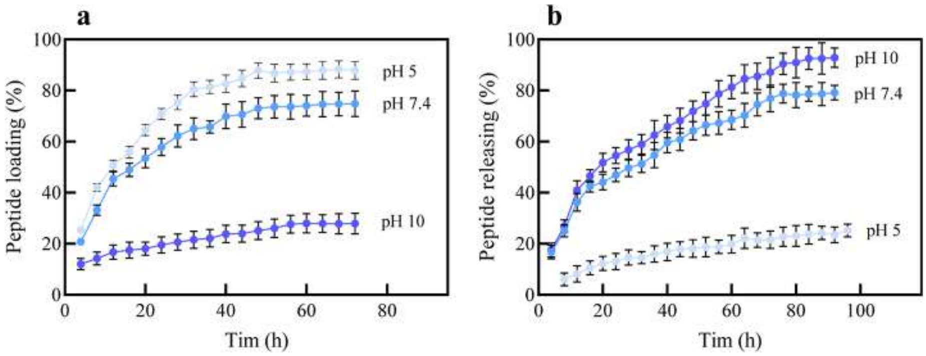

Figure 4. Peptide profile and structure. (a) Peptide loading and (b) release assay with TNBSA.

Tensile Property. The mechanical properties of the nanofiber mats are presented in Figure 3a and Table 2. The PVA−CS mat showed a brittle-like behavior with a higher Young's modulus and lower elongation at break, which indicates increasing intramolecular and cross-link reactions in PVA−CS nanofibers. PVA−HA nanofiber demonstrated the highest elongation at break, which is related to the elastomer behavior of PVA−HA nanofiber mats. Long-range interaction between HA chains induces an irregularly tangled with a random coil structure; these coils, under tension, straighten out. When the tensile force is released, the elastomer structure returns to its initial coil status.[35]

Before forming new tissue, flexible scaffolding similar to skin architecture is essential for the attachment and growth of wound edge cells. The data demonstrate that the PVA−HA and PVA−CS lack sufficient mechanical strength and elasticity for wound dressings, but the PVA−HA−CS composite nanofibers exhibit a ductile behavior. The Young's modulus, ultimate strength, and toughness of the composite nanofibers were significantly increased. Young's modulus is the ability of a material to withstand changes in length during longitudinal tension or compression. Moreover, the toughness of the composite mate showed about 7−13 times higher value (∼66−82 kN/mm), which could be a good candidate for fabricating skin substitution mats with much better flexibility. The effect of nanofiber thickness on mechanical properties has been eliminated through strain-stress diagram calculations.[36]

Degree of Citric Acid Cross-linking. The cross-linked nanofibers were fabricated through post-electrospinning heat treatment. The cross-linking densities of PVA−CS, PVA−HA, and PVA−HA−CS nanofibers were measured to be 93.38, 85.68, and 91.14%, respectively. The high cross-linking degree of nanofibers provided better structural stability in aqueous solutions for wound healing applications.

Surface Wettability. It is noteworthy that the amount, nature, and conformation of the absorbed proteins enormously affect the subsequent phase of wound healing.[37] It can be seen in Figure 3b that the contact angles of PVA−CS, PVA−HA, and PVA−HA−CS nanofibers before cross-linking were found to be 87.89, 34.99, and 75.14°, respectively. This high contact angle and low hydrophilicity are undesirable for medical applications, and non-cross-linked nanofibers quickly disappear when exposed to an aqueous solution. An ideal wound dressing should be highly able to absorb wound exudates and retain moisture in the wound environment. The decrease in the contact angle after cross-linking is most likely due to the presence of residual carboxyl groups of citric acid.

The results showed that cross-linking of nanofibers with citric acid not only protects nanofibers from disappearing in aqueous solutions but also improves the hydrophilicity characteristics of nanofibers for medical applications. These improvements were conducive to cell adhesion, proliferation, and protein adsorption.

In Vitro Degradation and Swelling Ratio. The degradation properties of a scaffold are crucial for the design of tissue-engineered constructs. As shown in Figure 3c, the PVA−CS and PVA−HA scaffolds have lost approximately 11 and 40% of their initial weight for 7 days, which is not compatible with skin tissue engineering purposes. The higher degradation rate of PVA−HA nanofibers is due to the high water absorption capacity of the HA polymer and the lowest cross-link density. But in the case of PVA−CS nanofibers, the lower degradation rate is ascribed to the higher cross-linking density. The biomaterials should degrade gradually rate along the tissue growth. Data demonstrated that PVA−HA−CS composite nanofiber had lost 26% of its initial weight in the same period, which is more compatible with the wound healing process.

The rate of diffusion of nutrients and absorb wound exudation fluid in nanofibers depends on the swelling behavior of the scaffold. As shown in Figure 3d, the scaffolds gained PBS 1.3−2.7 times their weight in the first 15 min of the experiment. The high degree of swelling observed at the PVA−HA−CS mate was due to the large quantity of water absorbed by the highly porous structure. The rapid and higher-magnitude swelling is quickly hydrated to prevent tissue adhesions.

Porosity and Pore Size Distribution. From the wound healing point of view, pore size and porosity of the nanofiber scaffold influence cellular attachment and proliferation behavior.[38] Figure 3e,f displays the relationship between porosity and pore size (fiber diameter) of nanofibers spun by different compositions. It was found that the PVA−HA−CS fiber exhibits a highly porous structure with a pore size of approximately 400 nm. These porous scaffolds can provide diffusion of gases and nutrients, structural space for cell attachment, and migration and metabolic waste removal.

ζ Potential of the Nanofiber. The surface charge of the scaffold is a crucial factor in the surface adsorption efficiency of biomolecules. The obtained data from the ζ potential measurements demonstrate that the surface ζ potential of the PVA−HA−CS nanofiber is approximately −30 mV in the pH range of 5−10 due to ionized groups on the surface (Figure 3g). The HA carboxylic group has a pK_a value of about 3.0, and therefore, at a pH greater than 3, the carboxylic groups of D-glucuronic acid are completely ionized. At this range of pH, the primary amine of CS polymer (pK_a = 6.5) is uncharged.

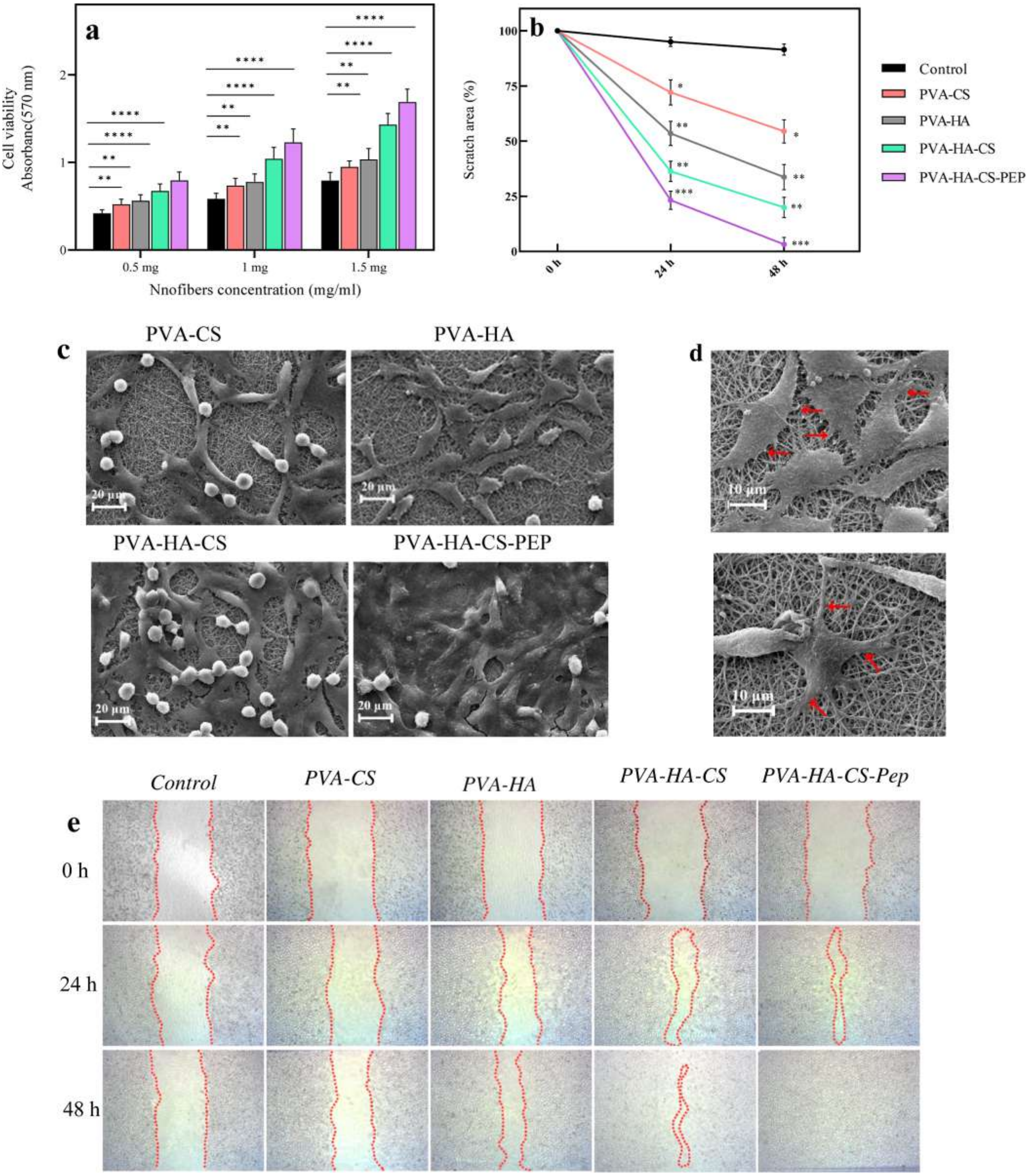

Figure 5. In vitro assay. (a) Cell proliferation (MTT) assay of L929 cultivated on electrospun nanofiber scaffolds at different concentrations (0.5, 1, and 1.5 mg/mL) and their proliferation potential compared with the control group, (b) quantitative analysis of wound closure as a function of time. The wound area was determined as the wound area at a given time relative to the original wound area, (c) SEM images of L929 cells grown on different electrospun nanofibers, (d) SEM images of L929 cell growth on a peptide-loaded nanofiber. Cells extend large lamellipodia and numerous filopodia, forming a branched network to anchor the cells to the substratum, (e) illustrative micrograph of cell migration into a scratch area over 24 and 48 h period after PVA−CS, PVA−HA, PVA−HA−CS, and PVA−HA−CS−PEP nanofiber treatment and.

Peptide Loading and Release. Characterization of the synthesized scaffolds demonstrated that the PVA−HA−CS nanofibers had optimized features for peptide loading. The efficiency of temporin-Ra immobilization into scaffolds was evaluated by the TNBSA method. TNBSA is a rapid and sensitive assay reagent for the determination of free amino

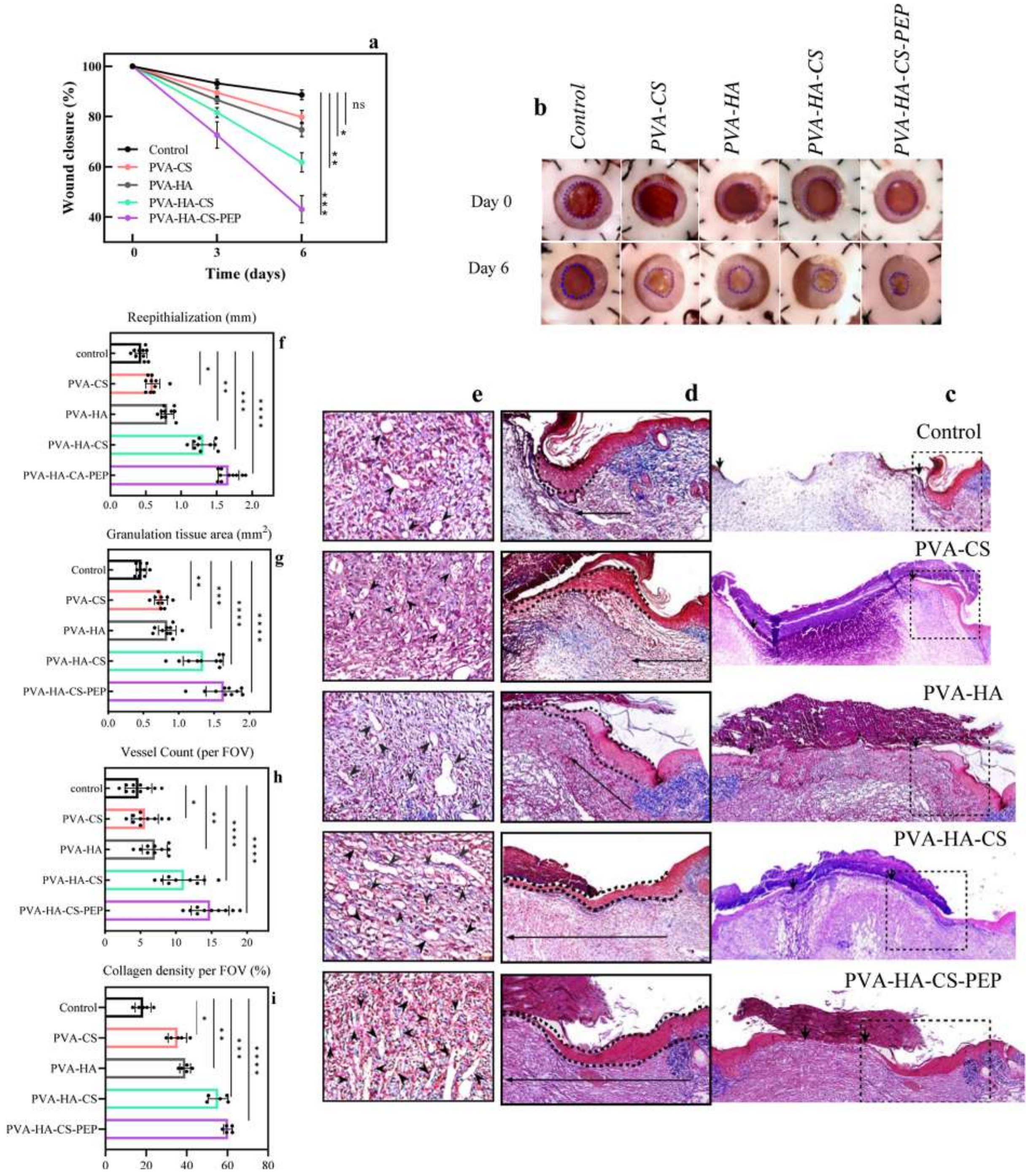

Figure 6. In vivo assay of nanofiber mats. (a) Time-dependent changes in the wound area determined with ImageJ analysis software (b), images of wound healing with different treatment groups on days 0 and 6, (c) histological analysis of the wounds 6 days after nanofiber treatment and representative image after Masson's trichrome staining of full-length transverse wound sections. A black arrowhead in histological sections indicates the wound edge, (d) the inset high-power images indicate the epithelial tongues (surrounded by the dotted black lines) and granulation tissue deposition (black arrows) of the wounds. (e) High-magnification histology images identifying blood vessels in the granulation tissue (arrows indicate blood vessels), (f–i) histomorphometry area of re-epithelialization, granulation tissue, blood vessel count based on fields of view (FOVs), and collagen density of wounded skin 6 days after treatment.

groups. Primary amines, upon reaction with the TNBSA reagent, form a highly chromogenic derivative, which can be measured at 335 nm.[39] Figure 4a shows that the loading of temporin-Ra increased from 27 to 87% as the pH value decreased from 10 to 5.

Furthermore, the simulation of the peptide structure in an aqueous medium with GROMACS software shows that the temporin-Ra peptide has two charged amino acids on its surface (Lys 3 and Lys 11), and the isoelectric point of temporin-Ra is around pH 10. In other words, when the pH value is less than 10, the temporin-Ra peptide becomes positively charged. Zeta potential studies showed that PVA−HA−CS nanofibers have a negative surface charge at pH less than 10. Therefore, peptide immobilization can be explained in terms of the electrostatic interaction between the negatively charged PVA−HA−CS scaffold and the positively charged peptides. At low pH, amine protonation increased peptide net charge (solubility) and enhanced peptide loading efficiency (Figure 4a). The release profile of the temporin-Ra peptide from PVA−HA−CS nanofiber was evaluated by immersing peptide-loaded nanofiber in PBS solutions at different pHs. As can be seen in Figure 4b, peptides were released faster from nanofiber in an alkaline environment (pH = 10) than at pH = 5 because the positive charge of the peptide was significantly reduced and, as a result, the electrostatic interaction between the peptide and the nanofiber functional groups was destroyed.

These results clearly show that the PVA−HA−CS nanofiber mat showed a significant peptide loading of 70% on the first day, which may be attributed to the high water uptake of nanofibers. In contrast, peptide release has occurred at a slower rate, possibly due to the formation of electrostatic interactions between polar amino acids such as lysine of peptides and functional groups of biopolymers. Gradual release prevents peptide aggregation and inactivation and promotes wound healing phases.

Cytocompatibility Assay of Fabricated Nanofibers. Viability and cell adhesion were analyzed using the MTT absorbance and SEM images of L929 cultured on the scaffolds. The MTT assay results (Figure 5a) demonstrated that, as the concentration of nanofibers increased from 0.5 to 1.5 mg/mL, cell proliferation also increased, and there was a notable difference between the control and nanofiber-treated cell proliferation rates. Cell proliferation assays suggested that all the nanofiber scaffolds were cytocompatible, and the proliferative capacity of fibroblast cells on PVA−HA−CS peptide-loaded nanofibrous scaffolds was significantly higher than that of the other groups. Other studies have confirmed the effect of antimicrobial peptides on the proliferation of fibroblast cells.[40,41] Cell adhesion exceedingly affects cell proliferation, differentiation, and migration. SEM image evaluation has revealed that (Figure 5c,d) the cells were flattened and well-spread on the surface of nanofibers. The cell filopodia spreading was strongly influenced by the surface characteristics of nanofibers, such as wettability, charge, topography, and rigidity. Biomaterials with hydroxyl, amine, and carboxyl functional groups are suitable for cell adhesion and proliferation.[42] The SEM micrographs indicated the highest adhesion and spread of cells on peptide-loaded nanofiber.

In Vitro Scratch Assay. From a tissue engineering perspective, cell migration ability on the surface of the synthesized scaffold is a critical feature in wound regeneration. After 48 h of treatment, the percentages of the wound area for the control, PVA−CS, PVA−HA, PVA−HA−CS, and PVA−HA−CS-PEP nanofiber mats were 91 ± 1, 54 ± 2, 33 ± 2, 20 ± 2, and 3.2 ± 1%, respectively. It is evident from Figure 5b that the peptide-loaded scaffold significantly accelerated the wound regeneration compared with other groups, which may be attributed to the localized release of the peptide from nanofibers and stimulation of cell migration using cell chemotaxis advantage.

In Vivo Wound Healing Study. The mouse excisional wound splinting model was used to assess the capabilities of different nanofibers in wound healing. Skin contraction is the principal mechanism of rodent wound healing. To create a humanized skin wound in the mouse, we have utilized a splinted excisional wound model.[43] In this study, the control group was not treated with nanofiber or other material. The wound surface was covered with Tegaderm for wound protection against pathogens. The rate of wound closure was measured on days 3 and 6, and the results are summarized in Figure 6b. After 6 days, the closure wound in the PVA−CS, PVA−HA, PVA−HA−CS, and PVA−HA−CS−PEP nanofibers reached 20, 25, 38, and 60%, as compared to 12% observed in the control group, respectively. The velocity of wound regeneration in the peptide-loaded group was considerably better than in the other groups (Figure 6a). Wound pH assay demonstrated that 12 h post-injuring, the pH value of the wound microenvironment increased from 5 to around 9. An increase in pH accelerated peptide release from the synthesized scaffold.

Histological Analysis. Wound healing is a complicated and dynamic process that overlaps the four stages of hemostasis, inflammation, proliferation, and remodeling. Successful completing of wound healing depends on performing various steps sequentially in the appropriate time frame.[44] Histological analysis was performed by Masson trichrome staining to provide a deeper understanding of the effectiveness of different nanofibers on wound healing, and the results are presented in Figure 6c.

Infiltration of polymorphonuclear inflammatory cells (PMNs) was elucidated in the control group, while the epithelial layer was not well developed. In comparison, the PVA−HA−CS−PEP dressing group showed fewer infiltrated PMNs than the control group. After PVA−HA−CS and peptide-loaded nanofiber treatment, the wound healing was significantly accelerated, and inflammatory cell filtration was decreased compared to the other group, which may be due to the synergistic anti-inflammatory effect of CS and HA. Previous studies showed that CS exerts immunomodulatory effects by releasing pro- and anti-inflammatory cytokines, chemokines, and growth factors via immune cells.[45] The compounds in the PVA−HA−CS−PEP scaffold are likely to accelerate the movement from the inflammatory phase to the proliferative phase of wound healing by triggering signaling pathways.[46] Re-epithelialization is characterized by forming a new epithelial layer and cellular migration. The epithelial barrier between the wound and the environment prevents tissue water loss and pathogen contamination.[47,48] Figure 6d demonstrates an increase in re-epithelialization at day 6 post-nanofiber treatment. The minimum rate of re-epithelialization was seen in the control group, while the peptide-loaded group exhibited the highest re-epithelialization rate after 6 days (Figure 6f,d).

Granulation tissue consists of a dermal matrix that provides a framework for cell migration.[49] The wounds treated with the peptide-loaded scaffold showed more granulation tissue formation compared with other groups; in contrast, the granulation tissue notably decreased in the control groups. The newly formed granulation tissue requires a vascular supply for its metabolic needs. Therefore, the designed scaffold for wound healing should potentially stimulate angiogenesis. High magnification (Figure 6e,h) was used to evaluate the number of blood vessels in the treated and control group. The highest blood vessel density was observed in PVA−HA−CS−PEP nanofiber. These results mainly agree with the granulation tissue-formation data (Figure 6g). Since collagen formation during wound healing supports fibroblast cell migration, reepithelization, and granulation process,[50] we evaluated collagen density in the wound area. As seen in Figure 6i, collagen density significantly increased in nanofiber peptide-loaded groups compared with the control group.

TNF-α Gene Expression Analysis. Previous studies show that TNF-a rapidly increased to the peak concentration level during the first several hours after wounding, and levels declined to the basal level.[51] Our data also confirmed the fluctuation of TNF-a cytokine production during the early stages of wound healing. As shown in Figure 7, the expression of TNF-α in the control group increased sharply after wounding, reached a peak level at 24 h, and returned to a basal level after 48 h. In contrast, once the mice were treated with the temporin-Ra peptide-loaded nanofiber, a peak level of TNF-α expression was observed 12 h after injury. The high-level expression of TNF-α returns to basal level at 24 h post-injury. The more prolonged inflammatory response of control groups suggests that the peptide may be responsible for the accelerated of inflammatory response of TNF-α at the earlier stage of the wound healing process.

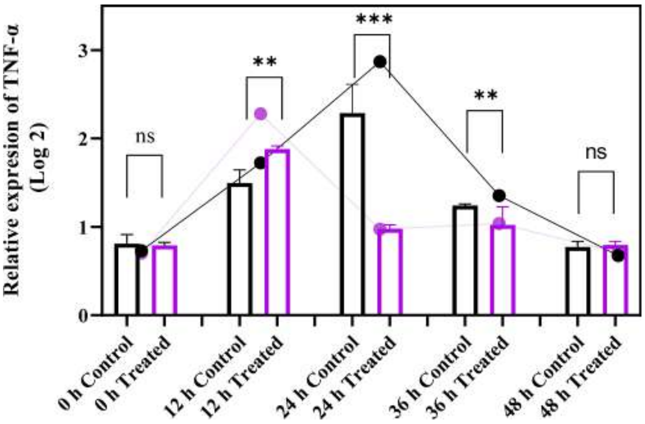

Figure 7. Effects of loaded peptide nanofiber treatment on the expression of TNF-α chemokine at a different time interval (0, 12, 24, 36, and 48 h after skin wounded).

CONCLUSIONS

AMPs are essential molecules in the innate immune system and regenerative processes. The peptide formulation to prevent their degradation and aggregation is a safe approach to implementing these biomolecules in medical engineering requirements. In this study, we have successfully designed pH-responsive nanofibrous scaffolds as a carrier for temporin-Ra antimicrobial peptides that can release peptides at the wound site. The immobilization via electrostatic interactions maintains the physiological activity of the peptides. According to the drug release profile and in vivo results, peptide release accrues in the alkaline environment of the wound. Physicochemical studies show that the PVA-HA-CS nanofiber had the uniform, bead-free, and interwoven morphology, similar to the ECM. Furthermore, synthesized nanofibers presented high wettability, swelling ratio, and porosity, which will further promise using the mats in skin substitution.

The in vitro study demonstrated that peptide-loaded nanofiber could positively enhance cell attachment, spreading, and proliferation, as well as promote cell−matrix interaction. Meanwhile, the histological analysis revealed that peptide-loaded dressings significantly accelerated wound closure and improved re-epithelialization of the wound area. Through the acceleration of the TNF-α cytokine response, the antimicrobial peptide promotes the inflammatory phase and thus increases the rate of wound healing. This study suggests the promising potential of a peptide-loaded nanofibrous mesh for effective wound healing. A unique feature of this nanofiber scaffold is the controlled release of the peptide and HA as the polymer slowly breaks down into smaller and non-toxic fragments during the wound healing process.

ASSOCIATED CONTENT

Supporting Information

The Supporting Information is available free of charge at https://pubs.acs.org/doi/10.1021/acsami.2c23268.

DSC heating scans of the PVA-CS nanofiber, PVA-HA nanofiber, PVA-HA-CS nanofiber, pure citric acid, chitosan, hyaluronic acid, and polyvinyl alcohol (PDF)

AUTHOR INFORMATION

Corresponding Author

Ahmad Asoodeh − *Department of Chemistry, Faculty of Science, Ferdowsi University of Mashhad, Mashhad 9177948974, Iran; Cellular and Molecular Research Group, Institute of Biotechnology, Ferdowsi University of Mashhad, Mashhad 9177948974, Iran*; orcid.org/0000-0002-1406-0595; Email: asoodeh@um.ac.ir

Author

Fatemeh Koohzad − *Department of Chemistry, Faculty of Science, Ferdowsi University of Mashhad, Mashhad 9177948974, Iran*

Complete contact information is available at: https://pubs.acs.org/10.1021/acsami.2c23268

Notes

The authors declare no competing financial interest.

ACKNOWLEDGMENTS

The authors appreciate the support provided by the Research and Technology Council of the Ferdowsi University of Mashhad, Iran (grant numbers: 3/47513 and 1397/06/27).

ABBREVIATIONS

PVA, polyvinyl alcohol
CS, chitosan
HA, hyaluronic acid
PEP, peptide

REFERENCES

(1) Thomas, S.; Grohens, Y.; Ninan, N. *Nanotechnology Applications for Tissue Engineering*; William Andrew, 2015.

(2) Youn, J.; et al. Thin and stretchable extracellular matrix (ECM) membrane reinforced by nanofiber scaffolds for developing in vitro barrier models. *Biofabrication* **2022**, *14*, 025010.

(3) Rathore, P.; Schiffman, J. D. Beyond the single-nozzle: Coaxial electrospinning enables innovative nanofiber chemistries, geometries, and applications. *ACS Appl. Mater. Interfaces* **2020**, *13*, 48−66.

(4) Luraghi, A.; Peri, F.; Moroni, L. Electrospinning for drug delivery applications: A review. *J. Controlled Release* **2021**, *334*, 463−484.

(5) Longinotti, C. The use of hyaluronic acid based dressings to treat burns: A review. *Burns Trauma* **2014**, *2*, 162.

(6) Kalva, S. N.; et al. Active agents loaded extracellular matrix mimetic electrospun membranes for wound healing applications. *J. Drug Delivery Sci. Technol.* **2021**, *63*, 102500.

(7) Nyman, E.; et al. Hyaluronic acid accelerates re-epithelialization and alters protein expression in a human wound model. *Plast. Reconstr. Surg.—Glob. Open.* **2019**, *7*, No. e2221.

(8) Castro, K. C.; Campos, M. G. N.; Mei, L. H. I. Hyaluronic acid electrospinning: Challenges, applications in wound dressings and new perspectives. *Int. J. Biol. Macromol.* **2021**, *173*, 251−266.

(9) Guo, X.; et al. Effects of chitosan oligosaccharides on human blood components. *Front. Pharmacol.* **2018**, *9*, 1412.

(10) Yilmaz Atay, H. Antibacterial activity of chitosan-based systems. *Functional chitosan*; Springer, 2019; pp 457−489.

(11) Antaby, E.; Klinkhammer, K.; Sabantina, L. Electrospinning of chitosan for antibacterial applications—Current trends. *Appl. Sci.* **2021**, *11*, 11937.

(12) Asoodeh, A.; Zardini, H. Z.; Chamani, J. Identification and characterization of two novel antimicrobial peptides, temporin-Ra and temporin-Rb, from skin secretions of the marsh frog (Rana ridibunda). *J. Pept. Sci.* **2012**, *18*, 10−16.

(13) Jatoi, A. W.; et al. Polyvinyl alcohol nanofiber based three phase wound dressings for sustained wound healing applications. *Mater. Lett.* **2019**, *241*, 168−171.

(14) Takigawa, T.; Endo, Y. Effects of glutaraldehyde exposure on human health. *J. Occup. Health* **2006**, *48*, 75−87.

(15) Campa-Siqueiros, P.; et al. Nanofibers of gelatin and polivinyl-alcohol-chitosan for wound dressing application: fabrication and characterization. *Polímeros* **2020**, *30*, No. e2020006.

(16) He, X.; et al. A frog-derived immunomodulatory peptide promotes cutaneous wound healing by regulating cellular response. *Front. Immunol.* **2019**, *10*, 2421.

(17) Thapa, R. K.; Diep, D. B.; Tønnesen, H. H. Topical antimicrobial peptide formulations for wound healing: Current developments and future prospects. *Acta Biomater.* **2020**, *103*, 52−67.

(18) Sun, J.; Perry, S. L.; Schiffman, J. D. Electrospinning nanofibers from chitosan/hyaluronic acid complex coacervates. *Biomacromolecules* **2019**, *20*, 4191−4198.

(19) Hosseini, H.; et al. Electrospinning of polyvinyl alcohol/chitosan/hyaluronic acid nanofiber containing growth hormone and its release investigations. *Polym. Adv. Technol.* **2021**, *32*, 574−581.

(20) Hussein, Y.; et al. Electrospun PVA/hyaluronic acid/L-arginine nanofibers for wound healing applications: Nanofibers optimization and in vitro bioevaluation. *Int. J. Biol. Macromol.* **2020**, *164*, 667−676.

(21) Nataraj, D.; Reddy, R.; Reddy, N. Crosslinking electrospun poly (vinyl) alcohol fibers with citric acid to impart aqueous stability for medical applications. *Eur. Polym. J.* **2020**, *124*, 109484.

(22) Cui, Y.; et al. The nanocomposite scaffold of poly (lactide-co-glycolide) and hydroxyapatite surface-grafted with L-lactic acid oligomer for bone repair. *Acta Biomater.* **2009**, *5*, 2680−2692.

(23) Lu, W.-C.; et al. Synthesis of Water Resistance and Moisture-Permeable Nanofiber Using Sodium Alginate−Functionalized Waterborne Polyurethane. *Polymers* **2020**, *12*, 2882.

(24) Saragih, S. W.; Wirjosentono, B.; Eddiyanto, Y.; Meliana, Y. Influence of crosslinking agent on the morphology, chemical, crystallinity and thermal properties of cellulose nanofiber using steam explosion. *Case Stud. Therm. Eng.* **2020**, *22*, 100740.

(25) Sercan, D.; Altay, F. Investigation of Electrophoretic Mobility of Various Nanofibers in Ethanol or Water. *Turk. J. sci. technol.* **2021**, *16*, 269−274.

(26) Cetinkaya, T.; et al. Fabrication and characterization of zein nanofibers integrated with gold nanospheres. *LWT* **2022**, *155*, 112976.

(27) Shukla, V.; et al. Evaluation of pH measurement as a method of wound assessment. *J. Wound Care* **2007**, *16*, 291−294.

(28) Chen, Y.; Yu, Q.; Xu, C.-B. A convenient method for quantifying collagen fibers in atherosclerotic lesions by ImageJ software. *Int. J. Clin. Exp. Med.* **2017**, *10*, 14904−14910.

(29) Vítková, L.; et al. Electrospinning of hyaluronan using polymer coelectrospinning and intermediate solvent. *Polymers* **2019**, *11*, 1517.

(30) El-hefian, E. A.; Yahaya, A. H. Rheological study of chitosan and its blends: An overview. *Maejo Int. J. Sci. Technol.* **2010**, *4*, 210−220.

(31) Tahalyani, J.; Rahangdale, K. K.; K, K. The dielectric properties and charge transport mechanism of π-conjugated segments decorated with intrinsic conducting polymer. *RSC Adv.* **2016**, *6*, 69733−69742.

(32) Varma, R.; Vasudevan, S. Extraction, characterization, and antimicrobial activity of chitosan from horse mussel Modiolus modiolus. *ACS Omega* **2020**, *5*, 20224−20230.

(33) Carneiro, J.; et al. Development and characterization of hyaluronic acid-lysine nanoparticles with potential as innovative dermal filling. *Braz. J. Pharm. Sci* **2016**, *52*, 645−651.

(34) Yadav, M. D. Advanced nanocomposite ion exchange materials for water purification. *Handbook of Nanomaterials for Wastewater Treatment*; Elsevier, 2021; pp 513−534.

(35) Ouellette, R.; Rawn, J. Synthetic Polymers. In *Principles of Organic Chemistry*; Ouellette, R. J., Rawn, J. D., Eds., 2015; pp 397−419.

(36) Roylance, D. *Stress-strain Curves*; Massachusetts Institute of Technology study: Cambridge, 2001.

(37) Junkar, I. Interaction of cells and platelets with biomaterial surfaces treated with gaseous plasma. *Advances in Biomembranes and Lipid Self-Assembly*; Elsevier, 2016; pp 25−59.

(38) Elnakady, Y.; et al. Vascular tissue engineering using polycaprolactone nanofibrous scaffolds fabricated via electrospinning. *Sci. Adv. Mater.* **2015**, *7*, 407−413.

(39) Fields, R. [38] The rapid determination of amino groups with TNBS. *Methods in enzymology*; Elsevier, 1972; pp 464−468.

(40) Takahashi, M.; et al. The antimicrobial peptide human β-defensin-3 accelerates wound healing by promoting angiogenesis, cell migration and proliferation through the FGFR/JAK2/STAT3 signaling pathway. *Front. Immunol.* **2021**, *12*, 3745.

(41) Park, H.-J.; et al. Antimicrobial peptide KSL-W promotes gingival fibroblast healing properties in vitro. *Peptides* **2017**, *93*, 33−43.

(42) Černochová, P.; et al. Cell type specific adhesion to surfaces functionalised by amine plasma polymers. *Sci. Rep.* **2020**, *10*, 9357.

(43) Hu, M. S.; et al. An improved humanized mouse model for excisional wound healing using double transgenic mice. *Adv. Wound Care* **2018**, *7*, 11−17.

(44) Mercandetti, M.; Cohen, A. J. Wound healing and repair. *Emedicine* **2017**, *14*, 12−20.

(45) Fong, D.; Hoemann, C. D. Chitosan immunomodulatory properties: perspectives on the impact of structural properties and dosage. *Future Sci.* **2018**, *4*, FSO225.

(46) Euppayo, T.; et al. Effects of hyaluronic acid combined with anti-inflammatory drugs compared with hyaluronic acid alone, in clinical trials and experiments in osteoarthritis: a systematic review and meta-analysis. *BMC Musculoskeletal Disord.* **2017**, *18*, 387.

(47) Xu, J.; et al. Role of mesenchymal stem cells in diabetic wound healing. *Wound Healing, Tissue Repair, and Regeneration in Diabetes*; Elsevier, 2020; pp 555−578.

(48) Falanga, V. Bioengineered skin constructs. *Principles of tissue engineering*; Elsevier, 2020; pp 1331−1352.

(49) Jain, C. M.; et al. Exploring the use of herbal drugs and advanced supporting techniques for wound healing. *Bull. Natl. Res. Cent.* **2022**, *46*, 16.

(50) Mathew-Steiner, S. S.; Roy, S.; Sen, C. K. Collagen in wound healing. *Bioengineering* **2021**, *8*, 63.

(51) Ritsu, M.; et al. Critical role of tumor necrosis factor-α in the early process of wound healing in skin. *J. Dermatol. Dermatol Surg.* **2017**, *21*, 14−19.